
Article:
Al-Gailani, A orcid.org/0000-0001-9290-0636, Sanni, O orcid.org/0000-0002-3895-7532, Charpentier, TVJ et al. (4 more authors) (2021) Role of temperature, roughness and pressure in crystallization fouling from potable water on aluminium surface. Thermal Science and Engineering Progress, 23. 100911. ISSN 2451-9049

https://doi.org/10.1016/j.tsep.2021.100911

Role of Temperature, Roughness and Pressure in Crystallization Fouling from Potable Water on Aluminium Surface

Amthal Al-Gailani[1]*, Olujide Sanni[1], Thibaut V. J. Charpentier[2], Richard Barker[1], Richard Crisp[3], Jantinus H. Bruins[4] and Anne Neville[1]

[1] *School of Mechanical Engineering, University of Leeds, Leeds, LS2 9JT, England*

[2]*School of Chemical and Process Engineering (SCAPE), University of Leeds, Leeds, LS2 9JT, England*

[3] *Fernox Limited, Woking, Surrey, GU21 5RW, England*

[4]*WLN, Glimmen, 9756 AD, Netherlands*

Abstract

This work evaluates the influence of surface temperature, roughness and system pressure on the crystallization fouling from potable water on an aluminium substrate. Experiments were conducted using two apparatus; one for temperature and roughness tests and another setup for pressure investigations. The findings show that a porous film of aluminium oxide forms on the aluminium substrate under all test conditions. Both temperature and surface roughness enhance the fouling rate with no obvious changes in the structure of the fouling layer. However, magnesium-calcium deposits were observed at the early stages of surface deposition. System pressure reduces the resistance to heat transfer as well as the scale amount on the surface. Moreover, the increase in pressure produces composite fouling of magnesium carbonate and calcium carbonate.

Keywords: Fouling; Aluminium; Pressure; Potable water; Calcium carbonate; Heat transfer

1.Introduction

Formation of inorganic deposits associated with water heating processes in the heat transfer systems is one of the most complex operational challenges. When fouling layers form on a heat transfer surface in household and industrial appliances, heat transfer rate is impaired, hence retarding the efficiency of the heat transfer system [1-3]. Deposition of inverse solubility salts retards the performance of domestic appliances such as coffee makers, steam irons, dishwashers, boilers, washing machines and potable water distribution systems [4]. A reduction in heat transfer efficiency, blockage of pipes and hence increase in power consumption are problems mostly encountered in household devices

subjected to fouling [5]. The mitigation of the fouling impact can be achieved by manipulating the surface properties, water chemistry and operational conditions.

Aluminium is one common metal used in the fabrication of heat transfer surfaces in household devices and systems. It possesses the second highest thermal conductivity after copper, but is less expensive, with fair resistance to corrosion in aqueous environments encountered in household devices [6]. There have been few significant attempts in terms of investigating fouling tendency on an aluminium surface using potable water as the test fluid. Teng, et al. [7] carried out experiments to study mineral deposition on five different substrates (copper, aluminium, brass, carbon steel and stainless steel). They reported that the amount and thickness of the deposit on the aluminium substrate are the second highest after copper. It was found that the surface deposition is dependent on the surface material [8].

Water containing oxygen catalyses the corrosion reaction of aluminium metal. Oxygen in water bonds with aluminium forming a protective film of aluminium oxide which prevents further oxygen attack [9]. It has been reported that the thickness of aluminium oxide Al_2O_3 film that forms in water is about twice of that forms in the air [10]. The rate of oxygen attack on the metal increases with temperature. The oxidation on aluminium proceeds by formation of an amorphous layer which subsequently develops to a crystalline oxide depending on temperature and time [11]. Aluminium oxide films form in a porous structure consisting of discrete islands. As a result of the porous structure, the oxide layer is highly absorbent and thus prone to corrosion and fouling in aggressive conditions [12].

Temperature is one of the decisive crystallization parameters that manipulates both morphology and reaction kinetics [13, 14]. There are several investigations of inorganic scale formation and only a few studies have focused on the influence of surface temperature. In addition to the stability of different forms of calcium carbonate ($CaCO_3$) [15], temperature affects the solubility of salts, reaction kinetics and foulants transport rate [16, 17]. However, the effect of surface temperature on surface deposition associated with water evaporation has received little attention. The dependency of boiling condition on temperature affects the local supersaturation in the vicinity of the surface and vicinity of nucleating vapour bubbles [18]. At the tested temperatures, the deposition of calcite as a prevailing polymorph of $CaCO_3$ is expected. However, the presence of magnesium and sulphate may lead to formation of needle-like aragonite [2].

Another critical parameter in domestic and industrial systems is pressure that may affect the fouling process alongside the temperature. Studies have investigated the relationship between the system pressure and the formation of scale in the upstream oil and gas industry [19-21]. It has been reported that the boiling heat transfer coefficient is independent of pressure and vapor quality [22, 23]. Pressure in the household appliances reaches up to 12 bars due to the generation of steam. The pressure range in these systems is undoubtedly much lower than that in the oil industry.

The surface roughness was determined to exert a noticeable impact on the tenacity of the $CaCO_3$ deposits [24]. In the study of Keysar, et al. [25], the adhesion of calcite crystal on the rough mild steel surface was estimated to be as much as 30 times greater than that for a smoother surface. In terms of morphology, the scale layer on the smooth surface is about three times more porous than that formed on the rough surface. Later, Bohnet [26] reported that the induction time reduced by eight times when the mean roughness depth increased by 16 times. The scale particles form on the hills and in the valleys of surface texture (Fig. 1). The sharp tops of asperities promote the heterogonous nucleation by acting as sites for crystallization initiation [27].

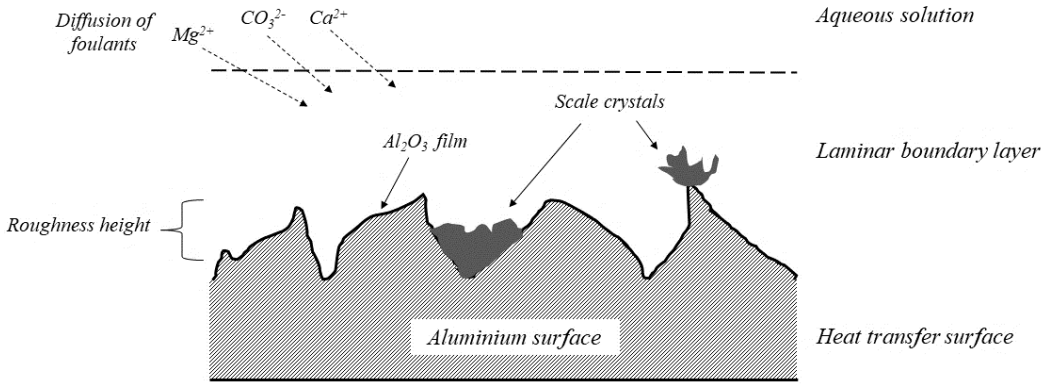

Fig. 1. Schematic representation of the fouling process on a rough aluminium surface.

The understanding of surface fouling from potable water in domestic appliances is a real challenge for the customers and manufacturers. For the better design of heat transfer surfaces, the effect of the key operating conditions and substrate needs to be studied. The present work is devoted to investigating the fouling process on the aluminium surface for different surface temperature, roughness and process pressure. The fouling evaluations include qualitative analysis (morphology) and quantitative measurement (fouling resistance and mass of deposits). The structure and composition of the oxide film formed on aluminium during the heating process were also examined. Two experimental setups were adopted in this study; the first setup for studying the influence of temperature and roughness, and the second one for pressure tests.

2.Experimental methods

2.1.Test solution

The solution used in the present experiment is a commercially available bottled water with pH of 7.2 and hardness of 3.07 mmol/L of $CaCO_3$, which is almost same as tap water hardness in some regions in the south UK. Table 1 lists the composition of the test fluid and initial saturation ratio to $CaCO_3$ as aragonite at 25 ℃. The analysis of the ionic species and pH measurements for the batch of bottled water used in the experiments were carried out.

Table 1. Composition of bottled potable water

Ion	mg/L
Ca^{2+}	85
Mg^{2+}	31
Na^{+}	6.5
K^{+}	1
Si^{4+}	15
HCO^{3-}	360
SO_4^{2-}	13
Cl^{-}	10
NO^{3-}	3.8
Dry residue at 180ºC	345
SR to aragonite $CaCO_3$	0.92

2.2.Experimental apparatus and procedure

2.2.1. Primary flow cell

The schematic diagram of the experimental setup is presented in Fig. 2. It comprises of a fresh solution tank, peristaltic pump, flow cell, heating system, data acquisition system and waste reservoir. The set-up is a once-through flow system that averts solution recirculation which may cause a decrease in supersaturation in the system over time. The primary flow cell, where surface scale forms, is built with an open-top window to work under atmospheric pressure (Fig. 3). A 10 mm thick nylon 6 material was used for the body part of the cell (130 mm length, 50 mm wide and 55 mm height). An aluminium sample is fixed by a nylon plastic holder located in the middle of the cell.

The test solution is placed in the feed tank at room temperature. The solution is fed to the flow cell using a peristaltic digital pump (MS-2/12 Reglo, Ismatec, Germany) at a controlled flow rate. The solution flows over the heated aluminium surface without fluid recirculation. As the experiments were performed at surface temperatures between 90-110 ºC, the test solution partially evaporates as a result of nucleate boiling condition. The generated steam leaves the cell through the top window, while the remaining liquid discharges to the waste tank. For all experiments, the flow rate was kept constant at 8 $ml.min^{-1}$.

Aluminium alloy 1050A (Al ≥ 99.5%) was used to fabricate test cylindrical specimen (22 mm height and 20 mm diameter). Aluminium was chosen as it is one of the most common materials used in constructing heat transfer surfaces in household appliances. The specimen was fabricated into a one-sided hollow cylinder with an inner diameter of 6.7 mm and depth of 19 mm (Fig.4). A bore enables to

firmly position a cartridge heater for heating the surface. A 3 mm depth channel was perforated in an internal wall to fit a K type temperature thermocouple between heater and specimen. The test specimen surface, which is the exposed surface to the solution was grounded with silicon carbide paper (1200 grit) and then polished with diamond suspension (0.5 μm). For the experiments to study the effects of roughness , the roughness grade of the test surface was obtained using silicon carbide papers and machining process. Thereafter, it was rinsed with acetone followed by distilled water and dried in an oven at 37 ℃ for 24 hours.

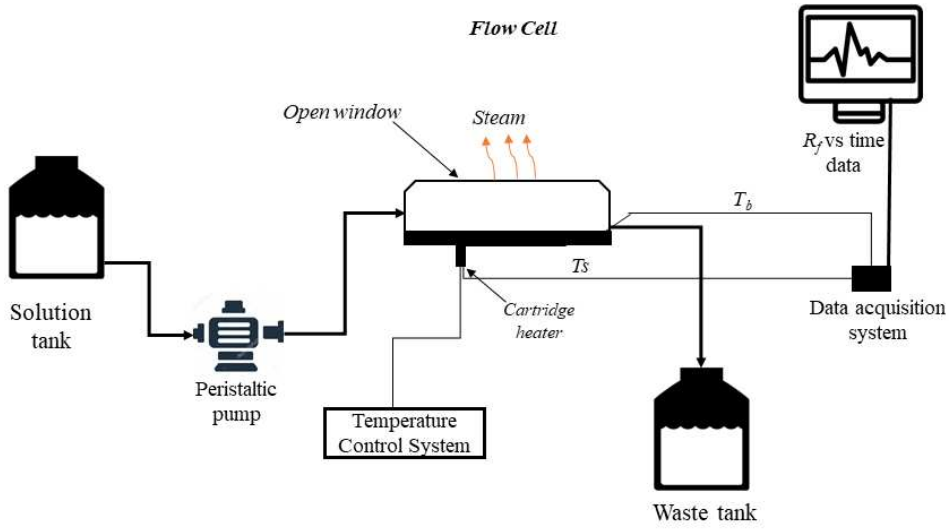

Fig. 2. Configuration of the experimental apparatus.

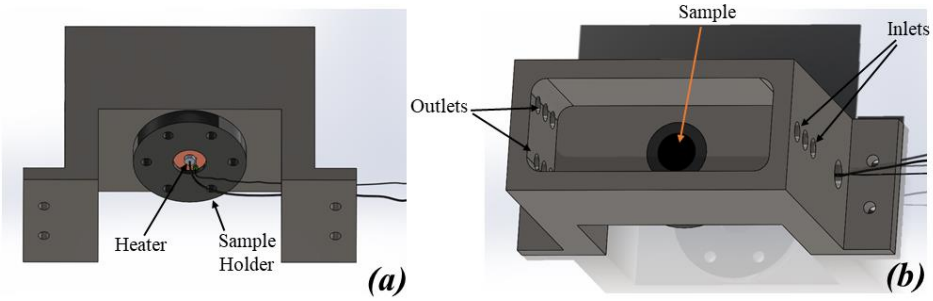

Fig. 3. The primary flow cell; (a) bottom view and (b) top view.

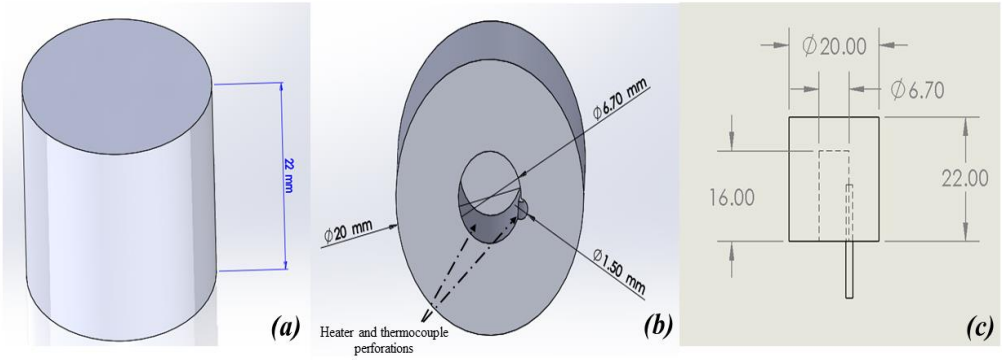

Fig. 4. The aluminium test sample; (a) top view, (b) bottom view and (c) 2D side view of assembly of thermocouple and sample (all dimensions in mm).

The insulating impact of the fouling layer on the heat flow was determined using thermal fouling resistance approach. The formation of salt deposits on the heat transfer surface raises the surface temperature and subsequently reduces the bulk temperature. Three mineral-insulated K type thermocouple sensors (TC Direct, UK) were adopted to measure the surface and bulk temperatures. These thermocouples were linked to a data acquisition system (NI USB-6009 multifunction I/O, UK) in which the analogue signals are converted into digital numeric values that are subsequently stored automatically. The fouling resistance is a measure of heat transfer retardation introduced by scale deposits. Fouling resistance was estimated using the following analytical expressions for convection heat transfer [28]:

$$R_f = \frac{1}{U_f} - \frac{1}{U_c} \quad \textbf{(1)}$$

$$R_f = \left(\frac{T_w - T_b}{Q}\right)_f - \left(\frac{T_w - T_b}{Q}\right)_c \quad \textbf{(2)}$$

$$R_f = \frac{T_w^f - T_w^c - T_b^f - T_b^c}{Q} \quad \textbf{(3)}$$

Where, U_c is the overall heat transfer coefficient for the clean surface, U_f is the overall heat transfer coefficient for the fouled surface, T_w is the surface temperature, T_b is the bulk temperature and Q is the heat flux. It is complicated to measure the bulk temperature at a certain point within the cell, as such, the average value of the inlet and outlet temperatures is considered. The fourth temperature thermocouple was placed in the channel between the heater and specimen to send feedback to the heating system which controls the temperature with an accuracy of ± 1 ℃. The heating system consists of a proportional–integral–derivative (PID) temperature controller (CAL 9900, UK) and stainless-steel cartridge heater (L: 25 mm, OD: 6.5 mm and power: 150 W).

2.2.2. Pressurized flow cell

The primary flow cell was modified to create a pressurized atmosphere in the cell. The steaming process inside the cell generates a pressure higher than the atmospheric pressure. A 3D-diagram of the modified pressurized flow cell is shown in figure 5. The body wall thickness of the primary cell was increased to 20 mm of Nylon 6 as a constructing material. The number of inlets and outlets was reduced to one each. The upper window was covered with a Nylon 6 lid (150 mm length, 70 mm wide and 10 mm height) which was attached to the body of the cell with stainless steel screws. A gasket made of rubber was placed between the lid and the cell to prevent potential leakage. No modifications were inserted on the specimen, specimen holder and heating system.

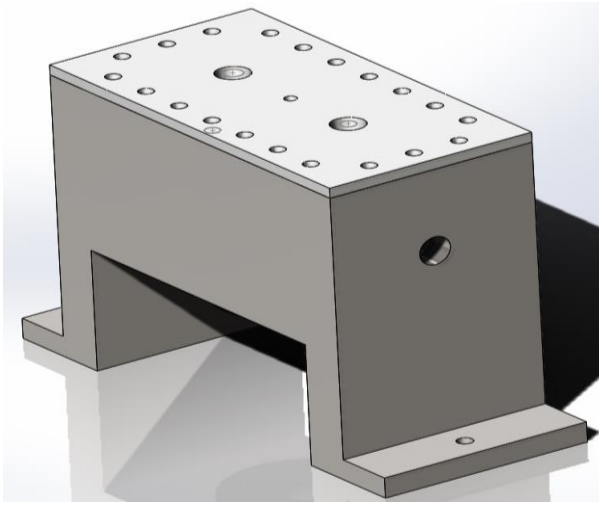

Fig. 5. Pressurized flow cell.

The experimental setup for pressure tests (Fig. 6) is different when compared with the configuration of the primary setup presented previously in Fig 2. For the pressure test, the test solution flows by the peristaltic pump to the cell in which solution evaporates and the formed steam generates pressure inside the cell. The pressure was measured using an analogue positive pressure gauge (RS components, UK). A pressure relief valve with a variable maximum set pressure was used to control the pressure. The solution flowing in the cell transforms completely to steam and batches through the relief valve, and liquid effluent is excluded. The exiting steam condenses in a plastic tube and flows to a waste tank. Temperature measurements were acquired and processed in the same procedure of the primary cell experiments. The experimental apparatus described herein mimics, to some extent, the steaming process in some domestic appliances, such as steam irons and boilers.

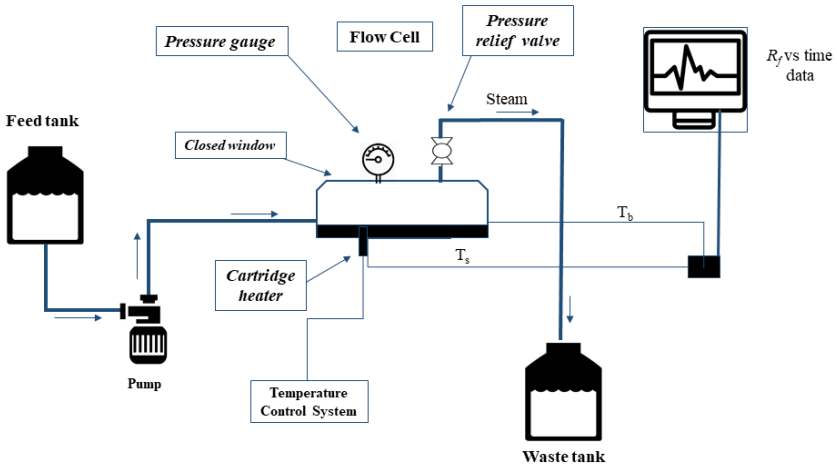

Fig. 6. Configuration of the experimental setup for pressure tests.

2.2.3. Solution and surface characterization

Prior to an experiment, the pH and ionic content of solution were evaluated using a pH-meter (HI 8014 Hanna, UK) and atomic absorption spectrophotometer (AAS) (Agilent Technologies, USA), respectively. The arithmetic average of the absolute values of the surface roughness (Ra) was measured using the 3D optical profiler NPFlex (Bruker, USA). A digital laboratory balance (Oxford GM2505D, UK) with an accuracy of ± 1.5 mg was utilized to weigh the specimen before and after a test.

For the post-experiment analysis, the fouled aluminium surface was rinsed with deionized water and later dried for 24 hours at 37 ºC in an oven. Scanning Electron Microscope (SEM) (Carl Zeiss EVO MA15) and a Field Emission Scanning Electron Microscopes (FE-SEM) (Hitachi SU8230) were used to examine the habit of the scale crystals. Elemental analysis of the deposit crystals was performed using an Energy-dispersive X-ray (EDX) (Oxford Instruments AZtecEnergy) with accelerating voltage of 15 kV and working distance between 9.2 to 10 mm. The X-ray diffraction (XRD) patterns for the scale layer were measured using a Philips X'Pert X-ray diffractometer (X'Pert MPD, Cu anode x-ray source, The Netherlands) with the 2 theta between 5 to 60º for 35 minutes at step size of 0.033 degrees. The experimental error bars were determined based on the standard deviation or difference between maximum and minumim values and the arithmetic mean. Experiments were conducted at least twice, and up to four times in some instances.

3. Results and Discussion

3.1.Aluminium oxide film

In all experiments of mineral scaling conducted on the aluminium surface at temperatures between 80 to 110 ºC, a thin passivation film of aluminium oxide fully covers the aluminium substrate (Fig. 7a). The scale crystals simultaneously grow through and on the aluminium oxide passive layer. Fig. 7 shows SEM and FE-SEM images of the aluminium oxide film at different magnifications. The oxide film comprises porous discrete islands distributed on the surface. The XRD analysis of the oxide layer shows that β-Al_2O_3 (beta alumina) is the dominant form of aluminium oxide on the substrate (Fig. 8).

Beta alumina has much lower thermal conductivity than that of bare aluminium surface which causes additional resistance to heat transfer [29]. The growth rate and thickness of the aluminium-oxide film increase as a function of substrate temperature [30]. The contact angle (CA) measurements show that the CA of the water droplet is 96º and 24º on a bare substrate and the oxide film respectively (Fig. 9). The formation of alumina film increases the hydrophilicity of the surface, essentially leading to higher crystal/substrate contact area. The hydrophilic surfaces are known to reduce the energy barrier for crystallization [31], hence higher fouling rate is expected on the alumina coated substrate [32]. Fouling rate is the amount of inorganic deposit formed on unit area of surface per unit time.

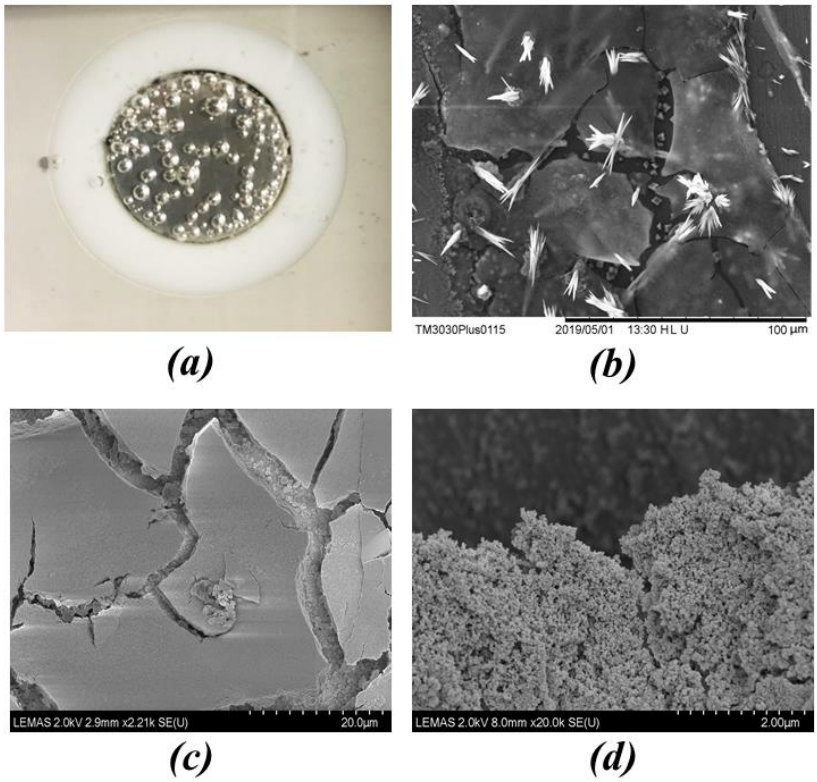

Fig 7. (a) Photo of aluminium surface coated with an aluminium oxide film, (b) SEM image of the oxide film segments with $CaCO_3$ crystals, (c) and (d) FE-SEM images of the oxide film with no scale crystals.

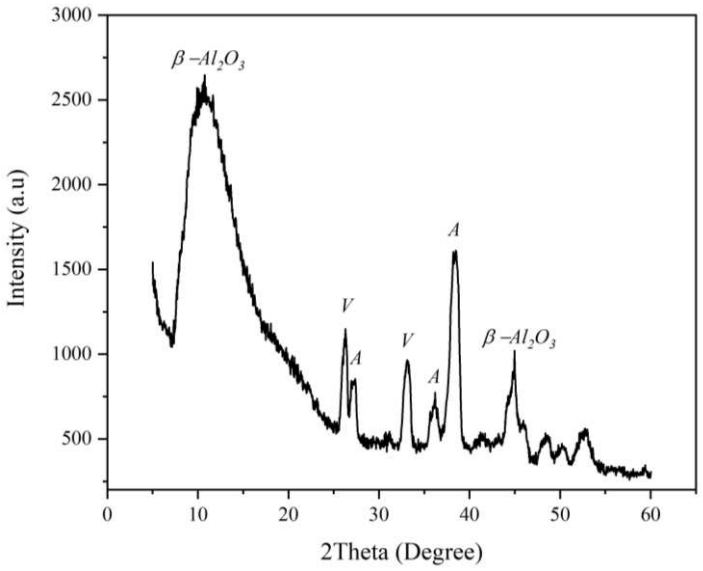

Fig. 8. XRD pattern of the aluminium oxide layer in presence of calcium carbonate particles [A: aragonite and V: vaterite].

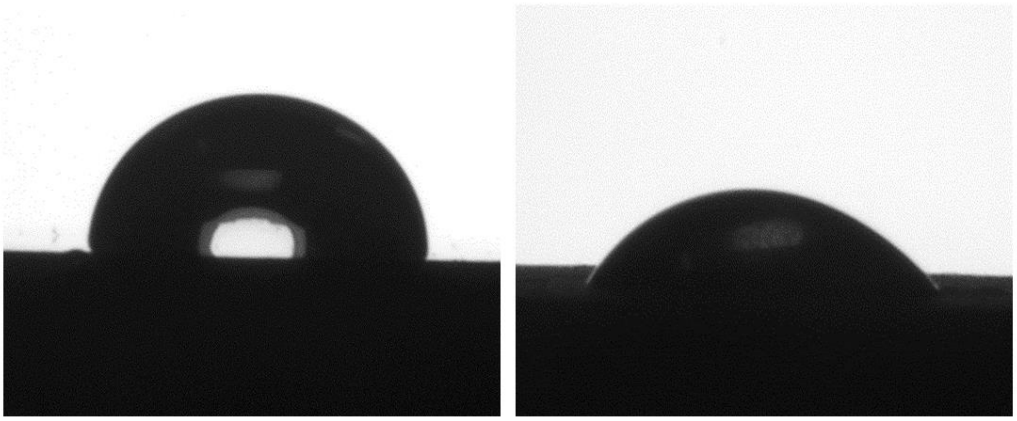

(a) *(b)*

Fig. 9. Contact angle measurement on (a) bare aluminium surface [96°] and (b) on aluminium oxide film [24°].

3.2.Effect of surface temperature

Figure 10(a) shows the effect of surface temperature on the thermal fouling resistance of the scale layer; temperature reduces the fouling induction period. Mullin [33] described induction time as the metastable state of supersaturated aqueous solution where spontaneous nucleation is not favourable. In all experiments, the heat transfer surface is fully covered with an inorganic fouling layer. The steady growth follows the induction period until reaches the asymptotic fouling resistance. The asymptotic fouling resistance increases with temperature increase (Fig. 10(b)). The asymptotic fouling resistance is attained when the deposition rate equals the removal rate. The surface temperature enhances the heterogeneous nucleation and growth rate of scale particles [34, 35]. The surface temperature reduces the local salt solubility at the vicinity of the surface.

The increase of surface temperature also promotes the vapour bubbles nucleation rate leading to increase in the interfacial concentration of fouling species. The fouling process in the vicinity of developing vapour bubbles is crystallization reaction controlled which is significantly affected by surface temperature [18]. These bubbles enhance the fluid turbulence near the surface, hence promote the heat transfer and reaction rate. The reduction in solubility and increase in concentrations both enhances the local supersaturation, which is the deposition driving force. The scale mass and the scale layer properties affect fouling resistance to heat transfer [36]. Fig. 10(b) demonstrates that the increase of fouling resistance is controlled by the mass of the deposit.

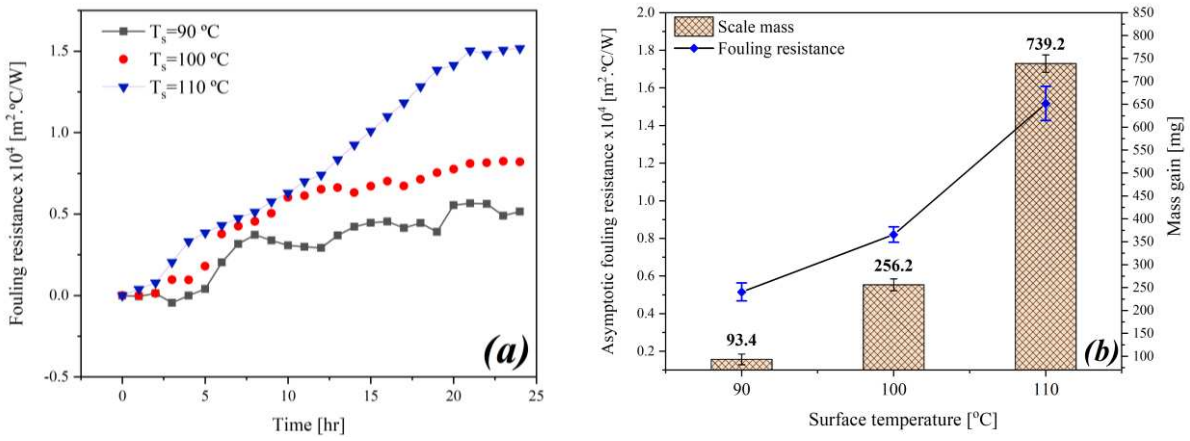

Fig. 10. (a) Thermal resistance of fouling layer on the aluminium surface, (b) surface mass gain and asymptotic fouling resistance, for different surface temperatures.

In terms of scale morphology, no significant differences in the size and shape of the deposited particles have been observed with increase in surface temperature (Fig. 11). The SEM image in Fig. 11(a) illustrates that the fouling layer at 90 ºC is the most porous. The needle-like aragonite is the predominant polymorphic phase of calcium carbonate at all tested temperature. Aragonite was reported as a metastable form of $CaCO_3$ under similar temperatures [37]. The SEM images for the surface at the early stages of crystallization show the different structure of the fouling layer (Fig. 12). The scale layer that formed in 2 hours of the experiment contains 14 wt.% of magnesium incorporated with calcium carbonate needles as shown by EDX analysis. These needles later grew to few micrometres after 22 hours of the experiment.

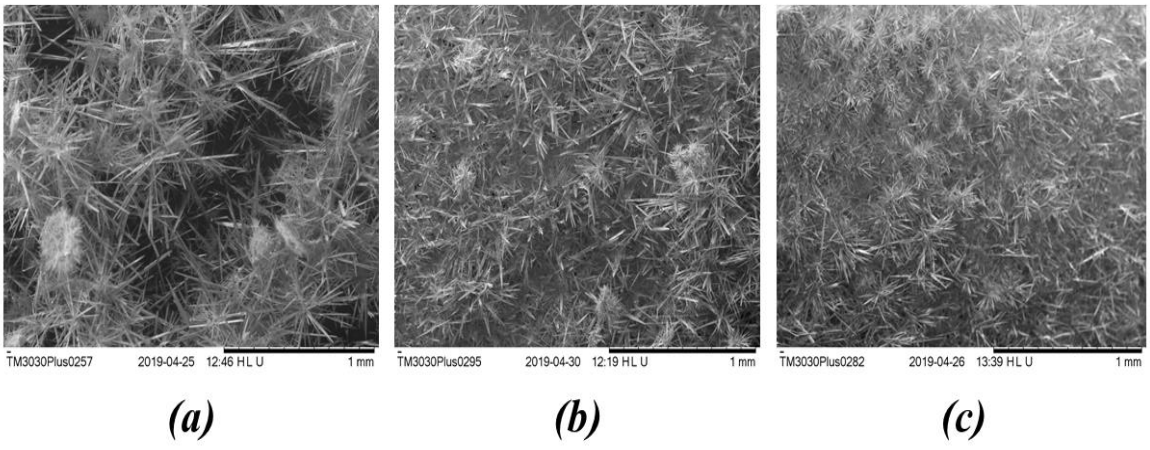

Fig 11. SEM images for deposits on the aluminium surface at different surface temperatures; (a) 90 ºC, (b) 100 ºC and (c) 110 ºC.

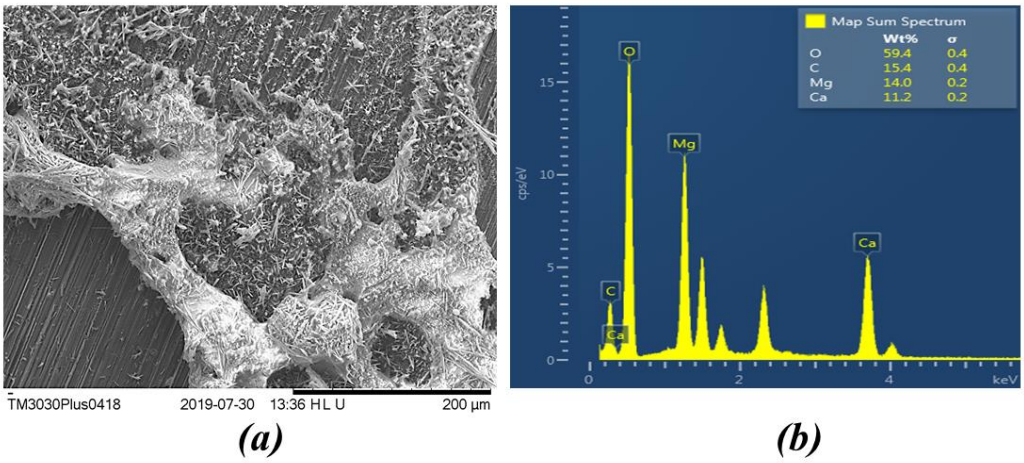

Fig 12. Deposits on the aluminium surface at 100 ºC; (a) SEM image and (b) EDX analysis.

3.3. Effect of pressure

Figure 13 displays the influence of pressure on the fouling resistance and the deposition rate. The pressure in the cell significantly minimizes the fouling resistance as well as the amount of the deposits. Relieving the pressure in the cell and discharging steam results in inconstancy in the fouling resistance curve. This might be attributed to the leaving vapour bubbles from the surface which enhance the heat transfer coefficient. An increase in pressure reduces the release of carbon dioxide from the solution. This shifts the equilibrium to the left-hand side, hence reducing the formation of $CaCO_3$ and $MgCO_3$ scale (Eqs. 4 and 5). Therefore, the effect of pressure on the scaling tendency of $CaCO_3$ is relatively significant [21].

$$Ca^{2+}_{(aq)} + 2HCO^{-}_{3\,(aq)} \leftrightarrow CaCO_{3\,(s)} + CO_{2\,(g)} + H_2O_{(l)} \quad \textbf{(4)}$$

$$Mg^{2+}_{(aq)} + 2HCO^{-}_{3\,(aq)} \leftrightarrow MgCO_{3\,(s)} + CO_{2\,(g)} + H_2O_{(l)} \quad \textbf{(5)}$$

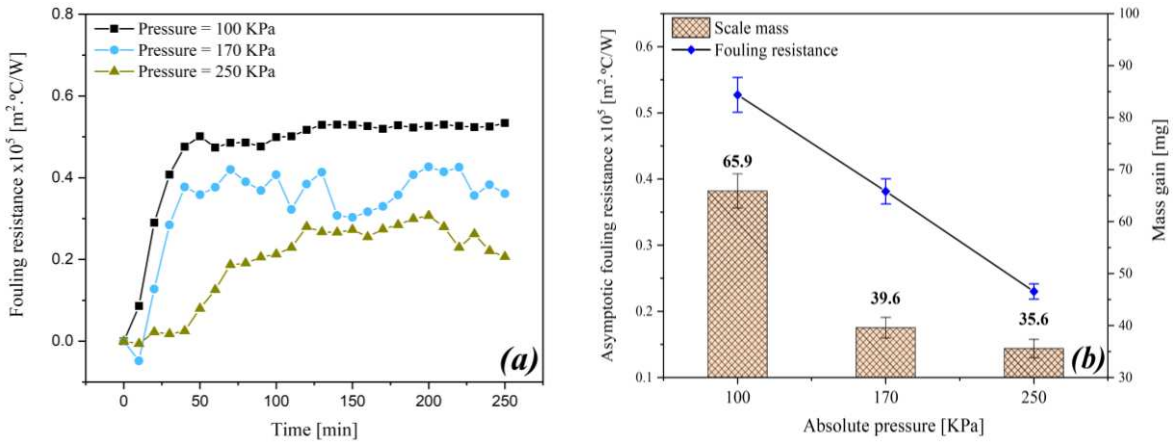

Fig. 13. (a) Thermal resistance of the fouling layer on the aluminium surface, (b) surface mass gain and asymptotic fouling resistance, for different absolute pressures.

Figure 14 shows SEM images of mineral deposits on the aluminium surface under different pressures. The salt particles aggregated in discrete colonies on the heat transfer surface. The salt crystals formed at a pressure of 100 kPa is a mixture of bouquet-like and dumbbell-like aragonite. As the pressure is increased to 170 kPa, more bouquet-like aragonite formed with flake-like $MgCO_3$. Spherical crystals of magnesium carbonate formed in aggregates with bouquet-like aragonite when the system is pressurized to 250 kPa. The presence of $MgCO_3$ in the fouling layer is suggested by EDX elemental measurement (Fig. 15). It is found that the crystals covered by spectrum A are $MgCO_3$ based empirical formula estimation from the quantities of each element, while spectrum B covers needles of $CaCO_3$. As pressure is increased, the deposition of magnesium carbonate is observed.

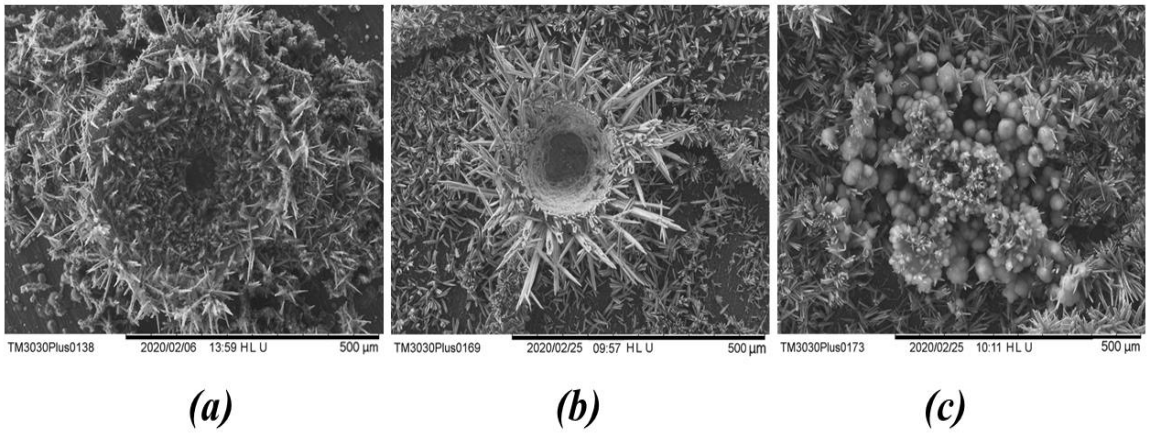

Fig 14. SEM images for deposits on the aluminium surface at different pressures; (a) 100 kPa, (b) 170 kPa and (c) 250 kPa.

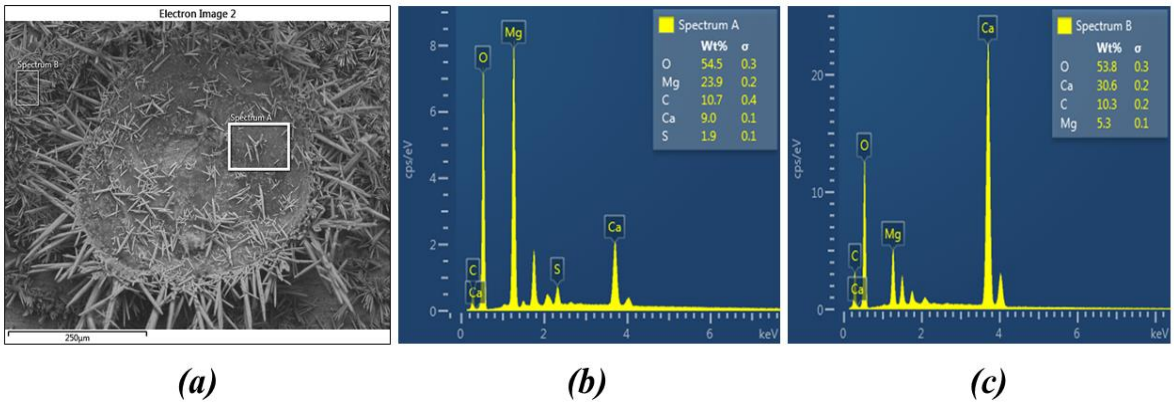

Fig 15. Deposits on the aluminium surface at 170 kPa; (a) SEM image, (b) Spectrum A (c) Spectrum B, from EDX analysis.

3.4. Effect of surface roughness

The influence of surface roughness on the heat transfer resistance of the fouling layer is presented in Fig. 16. The fouling resistance increases with increase in average surface roughness (R_a). Surface roughness exerts a noticeable impact on the rate of deposition. The profile element of the surface comprises asperities and valleys. The top sharp ends of asperities act as heterogonous nucleation sites which promote the scale particles formation [27] while the deep valleys protect the mineral deposition against the flow shear by acting as a shelter [26]. The unevenness of the rough surface provides a larger contact area developing the overall adhesion and tenacity of scale crystals [25]. For constant heat flux operation, an increase in roughness increases the surface heat transfer coefficient resulting in higher scale-solution interface temperature. In this case, the ageing rate decreases with slower reduction in the fouling resistance [38].

The amount of deposits increases with surface roughness increase (Fig. 16(b)). However, the amount of scale formed dropped from 403.3±15.8 mg to 396.4±17.6 mg when the roughness parameter increased from 1.18 to 1.48 µm. The reduction in the mass may owe to the change in the scale layer structure as the porosity of the fouling layer on a rough surface is relatively high [25]. The fouling layer comprises of different sub-layers [39], therefore, SEM technique is not adequately able to examine the salt layer porosity (Fig. 5). The SEM images in in figure 17 show minor differences in the scale morphology on different surface roughness. The surface texture of domestic appliances is a controllable parameter. Smoothing the pipe and pool surfaces reduces the scaling tendency of the potable water.

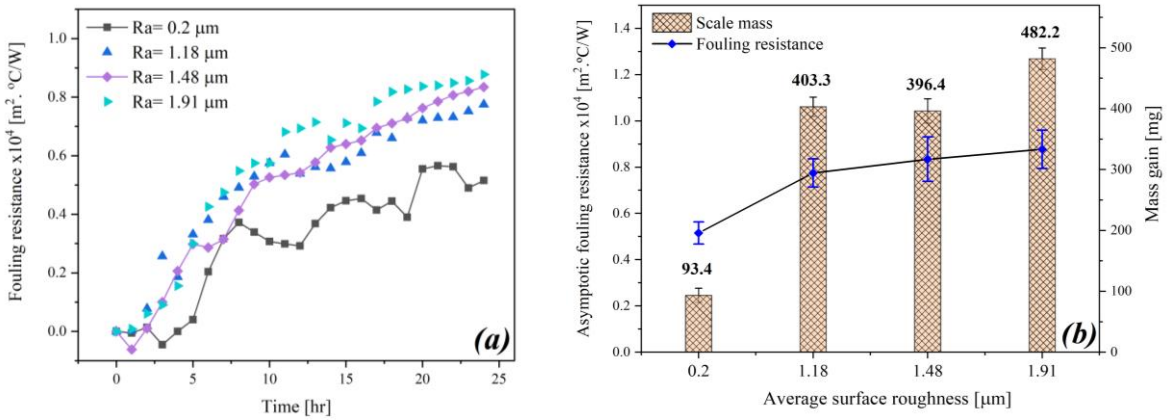

Fig. 16. (a) Thermal fouling resistance of scale on the aluminium surface, (b) surface mass gain and asymptotic fouling resistance, for different surface roughness.

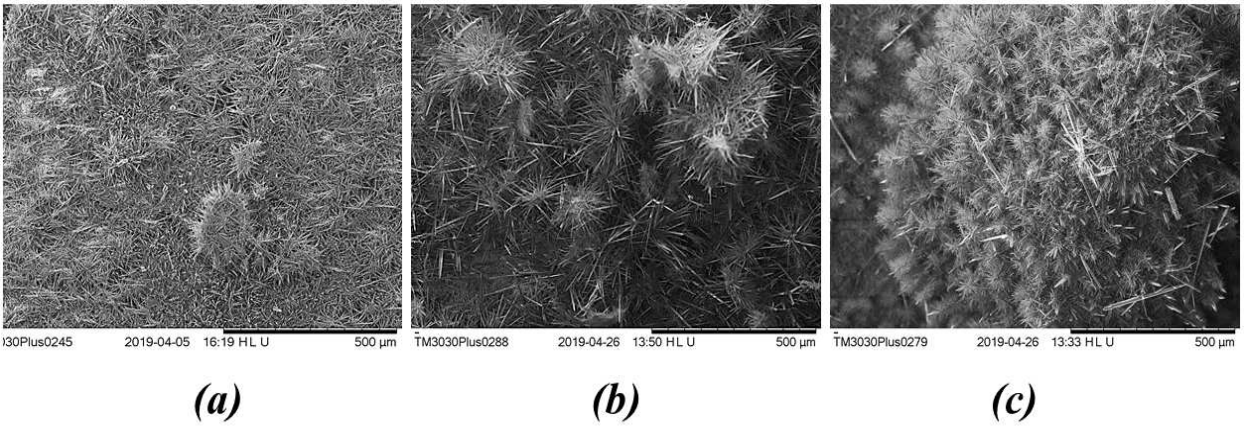

Fig 17. SEM images for deposits on the aluminium surface for different surface roughness; (a) R_a =1.18 µm, (b) R_a =1.48 µm and (c) R_a =1.91 µm.

The effect of minerals surface deposition has been evaluated using the thermal fouling resistance, the mass of scale and SEM-EDX analysis. These measurements are complementary by which some properties of the fouling layer can be estimated. Formation of different inorganic salts produces a composite layer on the heated surface which may result in variation in some properties such as thermal conductivity and density of the fouling layer. Therefore, comparing the fouling resistance with the mass of the deposits gives a good indication of how conductive the layer is, as illustrated in Equations 6 and 7 [40].

$$R_f = \frac{m_f}{\rho_f \lambda_f} \quad \textbf{(6)}$$

$$R_f = \frac{x_f}{\lambda_f} \quad \textbf{(7)}$$

Where, m_f is the fouling mass, ρ_f fouling layer density, λ_f is the fouling layer thermal conductivity and x_f is the layer thickness. For instance, the increase of ion content in the test fluid may reduce the fouling resistance with an insignificant change in the mass of deposits, as such, it can be inferred that the formed fouling layer is more conductive. The SEM observations provide knowledge of scale particle size, morphology and fouling layer porosity which enabled to further validate the findings from the fouling resistance and mass measurements.

Figure 18 illustrates the relationship between the asymptotic fouling resistance and fouling mass for the change in pressure, temperature and surface roughness. Asymptotic fouling resistance increases with the mass of deposits on the heated surface at all tested conditions. However, the change of system pressure produces a higher rise in the asymptotic fouling resistance when compared with temperature and roughness. This refers to that the fouling layer thermal conductivity, density or both decrease with the increasing pressure.

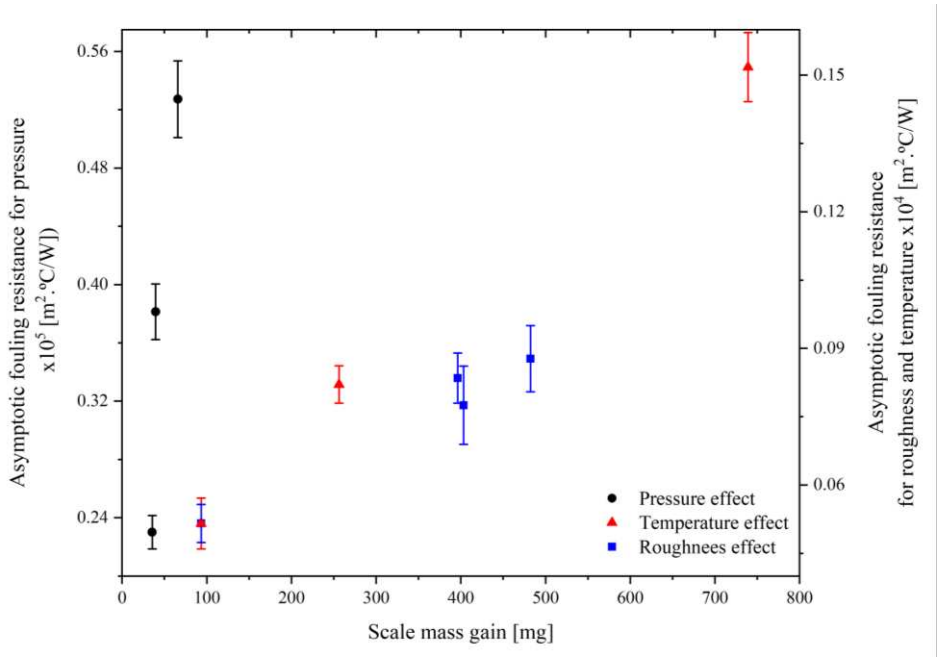

Fig. 18. The relationship between the fouling resistance and fouling mass.

4. Conclusions

Inorganic scale formation experiments were carried out on aluminium heat transfer surface from potable water. The tests, which were performed in two experimental setups, involve the study of the influence of surface temperature, roughness and system pressure. The key findings can be summarized as follows:

- During the water heating process using an aluminium substrate, a film of Al_2O_3 forms on the surface. The morphology analysis showed that the Al_2O_3 layer has a porous structure and good surface wettability.
- The temperature increases the fouling resistance and the amount of the deposits. Also, the increase in temperature produces less porous fouling layer. Needle-like aragonite is the prevailing deposition formed in all tested temperatures. In the early stages of surface scaling, magnesium containing deposits were detected on the surface.
- The pressure in the cell significantly minimizes the fouling resistance as well as the amount of the deposits. Pressure increase leads to the formation of separated colonies of $CaCO_3$ and $MgCO_3$ on the substrate.
- Surface roughness plays an important role in promoting the fouling rate. However, insignificant morphological changes were observed as a result of roughness increase.

Understanding the response of surface deposition process to different operating conditions and water chemistry helps to better design and improve the long term operation of domestic appliances.

Acknowledgement

The authors acknowledge the funding and support from the Leeds University SALSAS consortium. We also acknowledge the financial support of the Leverhulme Trust Research Grant ECF-2016-204. We also wish to acknowledge the technical and administrative team of the Institute of Functional Surfaces (IFS), School of Mechanical Engineering at the University of Leeds for their supports.

Nomenclature

$\boldsymbol{R}$	fouling resistance (m^2. K/W)
$\boldsymbol{U}$	overall heat transfer coefficient (W m^{-2} K^{-1})
$\boldsymbol{T}$	temperature (K)
$\boldsymbol{Q}$	heat flux (W/m^2)
$\boldsymbol{m}$	mass of scale (g)
$\boldsymbol{\rho}$	fouling layer density (g/m^3)
$\boldsymbol{\lambda}$	fouling layer thermal conductivity (W/m.K)
$\boldsymbol{x}$	fouling layer thickness (m)

Acronyms

SEM	Scanning Electron Microscopy
XRD	X-ray Diffraction
EDX	Energy Dispersive X-ray

Subscript/superscript

$\boldsymbol{f}$	fouled surface
$\boldsymbol{c}$	clean surface
$\boldsymbol{w}$	surface/ wall
$\boldsymbol{b}$	bulk

References

[1] A. Neville, "Surface Scaling in the Oil and Gas Sector: Understanding the Process and Means of Management," *Energy & Fuels,* vol. 26, no. 7, pp. 4158-4166, Jul. 2012. doi: https://doi.org/10.1021/ef300351w.

[2] A. Al-Gailani *et al.*, "Examining the effect of ionic constituents on crystallization fouling on heat transfer surfaces," *Int. J. Heat Mass Transfer,* vol. 160, p. 120180, 2020/10/01/ 2020. doi: https://doi.org/10.1016/j.ijheatmasstransfer.2020.120180.

[3] K. S. Song, J. Lim, S. Yun, D. Kim, and Y. Kim, "Composite fouling characteristics of CaCO3 and CaSO4 in plate heat exchangers at various operating and geometric conditions," *Int. J. Heat Mass Transfer,* vol. 136, pp. 555-562, 2019. doi: https://doi.org/10.1016/j.ijheatmasstransfer.2019.03.032.

[4] C. S. Richards, F. Wang, W. C. Becker, and M. A. Edwards, "A 21st-Century Perspective on Calcium Carbonate Formation in Potable Water Systems," *Environ. Eng. Sci.,* vol. 35, no. 3, pp. 143-158, Mar. 2018. doi: https://doi.org/10.1089/ees.2017.0115.

[5] S. N. Kazi, G. G. Duffy, and X. D. Chen, "Mineral scale formation and mitigation on metals and a polymeric heat exchanger surface," *Appl. Therm. Eng.,* vol. 30, no. 14, pp. 2236-2242, Oct. 2010. doi: https://doi.org/10.1016/j.applthermaleng.2010.06.005.

[6] P. A. Schweitzer, *Corrosion Engineering Handbook, -3 Volume Set*. CRC Press, 1996.

[7] K. Teng *et al.*, "Calcium carbonate fouling on double-pipe heat exchanger with different heat exchanging surfaces," *Powder Technol.,* vol. 315, pp. 216-226, Jun. 2017. doi: https://doi.org/10.1016/j.powtec.2017.03.057.

[8] J. Zhao, M. Wang, H. M. Lababidi, H. Al-Adwani, and K. K. Gleason, "A review of heterogeneous nucleation of calcium carbonate and control strategies for scale formation in multi-stage flash (MSF) desalination plants," *Desalination,* vol. 442, pp. 75-88, Sept. 2018. doi: https://doi.org/10.1016/j.desal.2018.05.008.

[9] N. Birbilis and B. Hinton, "19 - Corrosion and corrosion protection of aluminium," in *Fundamentals of Aluminium Metallurgy*, R. Lumley, Ed.: Woodhead Publishing, 2011, pp. 574-604.

[10] J. M. Bryan, "The action of boiling distilled water on aluminium," *Journal of the Society of Chemical Industry,* vol. 69, no. 6, pp. 169-173, Jun. 1950. doi: https://doi.org/10.1002/jctb.5000690603.

[11] L. P. H. Jeurgens, W. G. Sloof, F. D. Tichelaar, and E. J. Mittemeijer, "Structure and morphology of aluminium-oxide films formed by thermal oxidation of aluminium," *Thin Solid Films,* vol. 418, no. 2, pp. 89-101, 2002/10/15/ 2002. doi: https://doi.org/10.1016/S0040-6090(02)00787-3.

[12] J. Gonzalez, V. Lopez, A. Bautista, E. Otero, and X. Nóvoa, "Characterization of porous aluminium oxide films from ac impedance measurements," *J. Appl. Electrochem.,* vol. 29, no. 2, pp. 229-238, Feb. 1999. doi: https://doi.org/10.1023/A:1003481418291.

[13] K. Krömer *et al.*, "Scale Formation and Mitigation of Mixed Salts in Horizontal Tube Falling Film Evaporators for Seawater Desalination," *Heat Transfer Eng.,* vol. 36, no. 7-8, pp. 750-762, 2015/05/03 2015. doi: 10.1080/01457632.2015.954961.

[14] J. W. Morse, R. S. Arvidson, and A. Lüttge, "Calcium carbonate formation and dissolution," *Chem. Rev.,* vol. 107, no. 2, pp. 342-381, Jan. 2007. doi: https://doi.org/10.1021/cr050358j.

[15] Y. S. Han, G. Hadiko, M. Fuji, and M. Takahashi, "Factors affecting the phase and morphology of CaCO3 prepared by a bubbling method," *J. Eur. Ceram. Soc.,* vol. 26, no. 4-5, pp. 843-847, Jan. 2006. doi: https://doi.org/10.1016/j.jeurceramsoc.2005.07.050.

[16] F.-A. Setta, A. Neville, and H. J. Chen, "A surface kinetic scaling model for CaCO 3 on a stainless steel surface (316 L)," in *CORROSION 2012*, 2012: NACE International.

[17] M. B. Amor, D. Zgolli, M. Tlili, and A. Manzola, "Influence of water hardness, substrate nature and temperature on heterogeneous calcium carbonate nucleation," *Desalination,* vol. 166, pp. 79-84, Aug. 2004. doi: https://doi.org/10.1016/j.desal.2004.06.061.

[18] S. Najibi, H. Mu¨ ller-Steinhagen, and M. Jamialahmadi, "Calcium carbonate scale formation during subcooled flow boiling," 1997.

[19] C. Fan *et al.*, "Scale Prediction and Inhibition for Oil and Gas Production at High Temperature/High Pressure," *SPE-130690-PA,* vol. 17, no. 02, pp. 379-392, Jun. 2012. doi: https://doi.org/10.2118/130690-PA.

[20] A. V. García, K. Thomsen, and E. H. Stenby, "Prediction of mineral scale formation in geothermal and oilfield operations using the Extended UNIQUAC model: Part II. Carbonate-scaling minerals," *Geothermics,* vol. 35, no. 3, pp. 239-284, 2006/06/01/ 2006. doi: https://doi.org/10.1016/j.geothermics.2006.03.001.

[21] S. J. Dyer and G. M. Graham, "The effect of temperature and pressure on oilfield scale formation," *J. PETROL. SCI. ENG.,* vol. 35, no. 1-2, pp. 95-107, Jul. 2002. doi: https://doi.org/10.1016/S0920-4105(02)00217-6.

[22] K.-H. Bang, K.-K. Kim, S. Lee, and B. Lee, "Pressure effect on flow boiling heat transfer of water in minichannels," *International Journal of Thermal Sciences,* vol. 50, no. 3, pp. 280-286, 2011.

[23] M. Wambsganss, D. France, J. Jendrzejczyk, and T. Tran, "Boiling heat transfer in a horizontal small-diameter tube," 1993.

[24] D. E. Packham, "Surface energy, surface topography and adhesion," *Int. J. Adhes. Adhes.,* vol. 23, no. 6, pp. 437-448, Aug. 2003. doi: https://doi.org/10.1016/S0143-7496(03)00068-X.

[25] S. Keysar, R. Semiat, D. Hasson, and J. Yahalom, "Effect of surface roughness on the morphology of calcite crystallizing on mild steel," *J. Colloid Interface Sci.,* vol. 162, no. 2, pp. 311-319, Feb. 1994. doi: https://doi.org/10.1006/jcis.1994.1044.

[26] M. Bohnet, "Influence of the Transport Properties of the Crystal/Heat Transfer Surface Interfacial on Fouling Behavior," *Chemical Engineering & Technology,* vol. 26, no. 10, pp. 1055-1060, Oct. 2003. doi: https://doi.org/10.1002/ceat.200301807.

[27] W. Cheong, P. Gaskell, and A. Neville, "Substrate effect on surface adhesion/crystallisation of calcium carbonate," *J. Cryst. Growth,* vol. 363, pp. 7-21, Jan. 2013. doi: https://doi.org/10.1016/j.jcrysgro.2012.09.025.

[28] S. Krause, "Fouling of heat-transfer surfaces by crystallization and sedimentation," *International Chemical Engineering (A Quarterly Journal of Translations from Russia, Eastern Europe and Asia);(United States),* vol. 33, no. 3, Jul. 1993.

[29] P. J. Anthony and A. C. Anderson, "The Thermal Conductivity of β-Alumina," in *Superionic Conductors*, G. D. Mahan and W. L. Roth, Eds. Boston, MA: Springer US, 1976, pp. 371-372.

[30] L. P. H. Jeurgens, W. G. Sloof, F. D. Tichelaar, and E. J. Mittemeijer, "Growth kinetics and mechanisms of aluminum-oxide films formed by thermal oxidation of aluminum," *J. Appl. Phys.,* vol. 92, no. 3, pp. 1649-1656, Jul. 2002. doi: https://doi.org/10.1063/1.1491591.

[31] S. B. Subramanyam, G. Azimi, and K. K. Varanasi, "Designing Lubricant-Impregnated Textured Surfaces to Resist Scale Formation," *Advanced Materials Interfaces,* vol. 1, no. 2, p. 1300068, Jan. 2014. doi: https://doi.org/10.1002/admi.201300068.

[32] S. Dash, L. Rapoport, and K. K. Varanasi, "Crystallization-Induced Fouling during Boiling: Formation Mechanisms to Mitigation Approaches," *Langmuir,* vol. 34, no. 3, pp. 782-788, Oct. 2017. doi: https://doi.org/10.1021/acs.langmuir.7b02936.

[33] J. W. Mullin, *Crystallization*. Elsevier, 2001.

[34] D. Hasson, M. Avriel, W. Resnick, T. Rozenman, and S. Windreich, "Mechanism of calcium carbonate scale deposition on heat-transfer surfaces," *Industrial & Engineering Chemistry Fundamentals,* vol. 7, no. 1, pp. 59-65, Feb. 1968. doi: https://doi.org/10.1021/i160025a011.

[35] T. Pääkkönen, M. Riihimäki, C. Simonson, E. Muurinen, and R. Keiski, "Crystallization fouling of $CaCO_3$ –Analysis of experimental thermal resistance and its uncertainty," *Int. J. Heat Mass Transfer,* vol. 55, no. 23-24, pp. 6927-6937, Nov. 2012. doi: https://doi.org/10.1016/j.ijheatmasstransfer.2012.07.006.

[36] M. Mayer *et al.*, "Investigation and visualization of crystallization fouling in a micro heat exchanger," in *Proceedings of the 2nd European Conference on Microfluidics, Toulouse, France*, 2010.

[37] K. N. Islam *et al.*, "Characterisation of calcium carbonate and its polymorphs from cockle shells (Anadara granosa)," *Powder Technol.,* vol. 213, no. 1-3, pp. 188-191, Nov. 2011. doi: https://doi.org/10.1016/j.powtec.2011.07.031.

[38] E. M. Ishiyama, F. Coletti, S. Macchietto, W. Paterson, and D. Wilson, "Impact of deposit ageing on thermal fouling: lumped parameter model," *AlChE J.,* vol. 56, no. 2, pp. 531-545, 2010.

[39] F. Brahim, W. Augustin, and M. Bohnet, "Numerical simulation of the fouling process," *International Journal of Thermal Sciences,* vol. 42, no. 3, pp. 323-334, Mar. 2003. doi: https://doi.org/10.1016/S1290-0729(02)00021-2.

[40] T. R. Bott, "CHAPTER 17 - Obtaining Data," in *Fouling of Heat Exchangers*, T. R. Bott, Ed. Amsterdam: Elsevier Science B.V., 1995, pp. 479-516.